nature materials

SUPPLEMENTARY INFORMATION

DOI: 10.1038/NMAT2747

A Single-Layer Wide-Angle Negative Index Metamaterial at Visible Frequencies

Stanley P. Burgos[1†], Rene de Waele[2†], Albert Polman[2], Harry A. Atwater[1*]

[1]*Kavli Nanoscience Institute, California Institute of Technology MC 128-95, Pasadena, CA 91125, USA*

[2]*Center for Nanophotonics, FOM Institute AMOLF Science Park 104, 1098 XG Amsterdam, The Netherlands*

[*] Corresponding author. E-mail: haa@caltech.edu
[†] These authors contributed equally to this work.

Supplementary Information Guide

Supplementary Figures and Legends S1-S6
These figures show the negative index mode field profiles and dispersion relations supported by the plasmonic coaxial waveguide geometry, and summarize the effective refractive index of the coupled plasmonic coaxial waveguide array for varying incident angle and array pitch.

Supplementary Discussion
This discussion explains the modal decomposition method for a single plasmonic coaxial waveguide.

Supplementary Movie S1
This movie shows backwards phase front propagation and negative refraction of λ_0 = 483 nm light incident at a 30° angle from air onto a semi-infinite NIM slab (QuickTime; 6.6MB).

Supplementary Movie S2
This movie shows negative refraction of λ_0 = 483 nm light incident on a ~300 nm thick NIM slab cut at a 3° angle (QuickTime; 1.3MB).

DOI: 10.1038/NMAT2747

Supplementary Information

Supplementary Figures and Legends

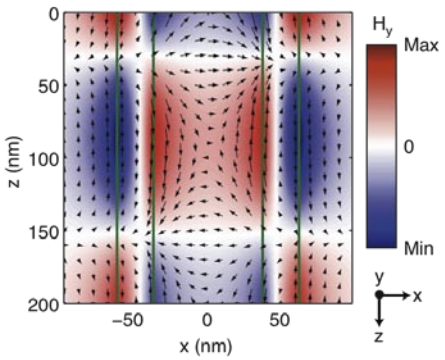

Figure S1. Coaxial waveguide negative-index mode. Lateral cross-section of a coaxial waveguide consisting an infinitely long 25 nm GaP annular channel with a 75 nm inner diameter embedded in Ag. The dielectric channel is schematically indicated. Plotted is the real part of the *H*-field distribution of the *n*=1 negative index mode at λ_0 = 483 nm, where *n* refers to the azimuthal dependence of the fields. The in-plane Re(H_{xz}) field distribution is depicted with arrows while the out-of-plane Re(H_y) fields are plotted using a color scale.

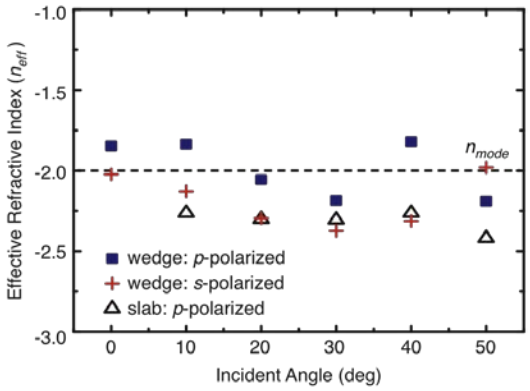

Figure S2. Summary of effective refractive index for varying angle of incidence. The metamaterial effective refractive index n_{eff} is plotted for λ_0 = 483 nm *s*- and *p*-polarized light incident at angles ranging from 0 − 50° derived from slab wave vector angles as in Fig. 3a as well as from refraction angle measurements in wedge-shaped samples as in Fig. 5. The dashed line indicates the calculated mode index of a single coaxial waveguide.

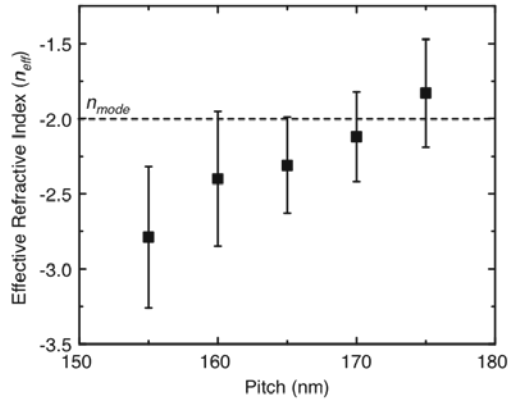

Figure S3. Effective refractive index as a function of pitch. The effective refractive index n_{eff} derived from wave vector angles is plotted as a function of pitch for λ_0 = 483 nm *p*-polarized light incident at 30° on a variable pitch waveguide array slab similar to that shown in Fig. 3a. The dashed line indicates the calculated mode index of a single coaxial waveguide.

DOI: 10.1038/NMAT2747

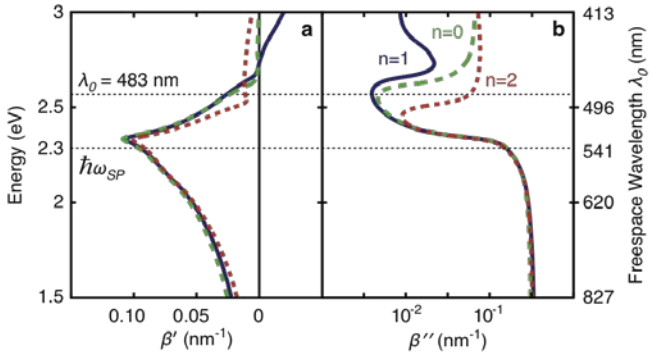

Figure S4. Coaxial waveguide mode dispersion relations. The coaxial waveguide consists of an infinitely long 25 nm GaP annular channel with a 75 nm inner diameter embedded in Ag. Plotted are the n = 0, 1, and 2 dispersion relations, where n refers to the azimuthal dependence of the fields in the waveguide described by the harmonic function $e^{in\psi}$ of order n. Energy is plotted versus β' in (**a**), β'' in (**b**). The Ag/GaP planar surface plasmon energy at $\hbar\omega_{SP}$ = 2.3 eV (λ_0 = 540 nm) and the target negative-index operation wavelength (λ_0 = 483 nm) are indicated by black dashed horizontal lines.

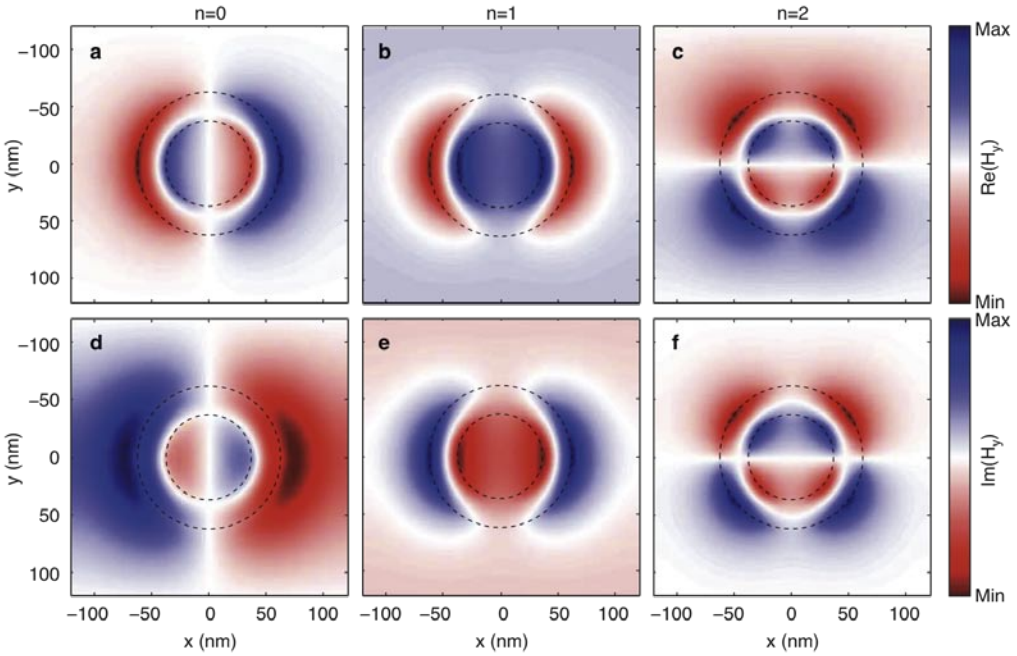

Figure S5. Coaxial waveguide eigenmodes. The coaxial waveguide consists of an infinitely long 25 nm GaP annular channel with a 75 nm inner diameter embedded in Ag. Plotted are the real (**a, b, c**) and imaginary (**d, e, f**) parts of the H_y field components of the n = 0 (**a, d**), 1 (**b, e**), and 2 (**c, f**) modes at λ_0 = 483 nm, where n refers to the azimuthal dependence of the fields.

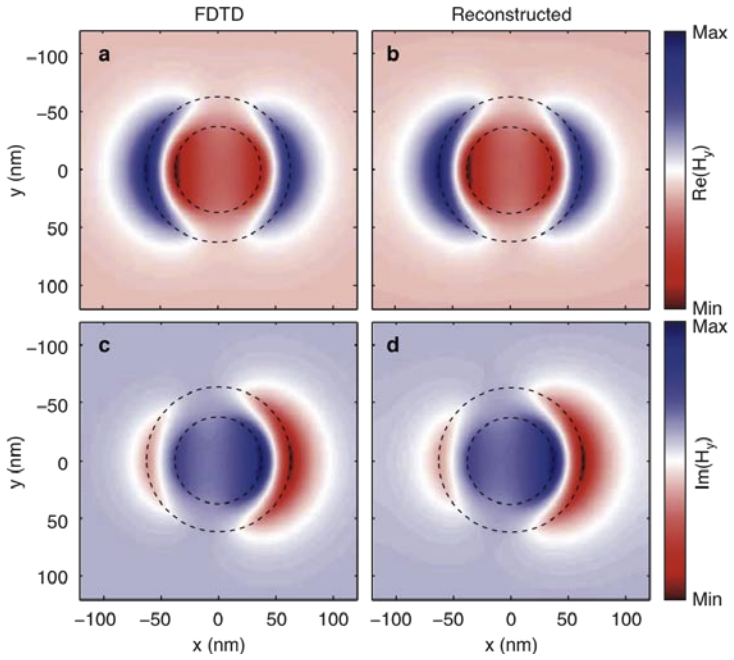

Figure S6. Modal reconstruction. A semi-infinite coaxial waveguide consisting of a 25 nm GaP annular channel with a 75 nm inner diameter embedded in Ag is illuminated from air with λ_0 = 483 nm light at a 50° angle-of-incidence. Plotted are the real and imaginary parts of H_y. The two panels on the left (**a, c**) show the mode excited inside the waveguide and the two right-side panels (**b, d**) show the mode reconstructed from a superposition of 87% n=1 mode and 13% n=0 mode, where n refers to the azimuthal dependence of the fields.

Supplementary Discussion

Modal decomposition. Conducting a modal decomposition on a single coaxial waveguide structure excited at the maximum incidence angle of 50° with λ_0=483 nm light, we find that the resulting excited waveguide mode is composed of 87% n=1 mode and only 13% n=0 mode, where n refers to the azimuthal dependence of the fields in the waveguide described by the harmonic function $e^{in\psi}$ of order n. The accuracy of the modal decomposition can be seen in Fig. S6 where the measured and reconstructed waveguide modes are plotted with 99.97% modal overlap. Furthermore, in looking at the dispersion relations of these two modes, we find that their complex indices are similar around the operation wavelength λ_0 = 483 nm (Fig. S4), thus explaining why the minor contribution from the n = 0 mode does not significantly affect the overall functionality of the predominantly n = 1 mode material at off-normal angles of incidence. For reference, H_y field cross-sections of the three lowest order modes (n = 0, 1, 2) are plotted in Fig. S5.

DOI: 10.1038/NMAT2747

Supplementary Movie Legends

Movie S1. Time evolution of the magnetic field distribution Re(H_y) along the polarization plane of a semi-infinite NIM slab excited with λ_0 = 483 nm *p*-polarized light incident at a 30° angle from air (Fig. 3a). The simulation geometry is schematically indicated. Playing the movie file forwards in time clearly shows that phase fronts inside the NIM have a negative phase velocity and refract negatively with respect to the surface normal.

Movie S2. Time evolution of the steady-state magnetic field distribution Re(H_x) along the plane of refraction for λ_0 = 483 nm *s*-polarized light at normal incidence to the right-angle side of a ~300 nm thick NIM slab cut at a 3° angle (Fig. 5a). The simulation geometry is shown schematically along with the surface normal of the output plane. Playing the movie forwards in time shows that light refracts negatively at the angled side of the prism due to the accumulation of negative phase across the wedge thickness.